

## COMPARISON OF *ASCA* AND *ROSAT* CLUSTER TEMPERATURES: A2256, A3558 AND AWM7

MAXIM MARKEVITCH<sup>1</sup>

University of Virginia, Astronomy Department, Charlottesville, VA 22903; mlm5y@virginia.edu

AND

ALEXEY VIKHLININ<sup>1</sup>

Harvard-Smithsonian Center for Astrophysics, 60 Garden St., Cambridge, MA 02138; alexey@head-cfa.harvard.edu

*Accepted for ApJ, 1996 July 24*

### ABSTRACT

We address the consistency between *ASCA* and *ROSAT* spatially-resolved cluster temperature measurements, which is of significant immediate interest given the recent *ASCA* reports of temperature gradients in several hot clusters. We reanalyze *ROSAT* PSPC data on A2256 (originally analyzed by Briel & Henry) using the newer calibration and a technique less sensitive to the calibration uncertainties. We find a temperature decline with radius in good agreement with *ASCA*'s, although with much larger errors than those of *ASCA*. We also present *ASCA* temperature maps and radial profiles of two cooler clusters, A3558 and AWM7. These are compared to the *ROSAT* results of Bardelli et al. and Neumann & Böhringer. In A3558, our analysis detects an asymmetric temperature pattern and a slight radial temperature decline at  $r \sim 0.5 h^{-1}$  Mpc, in addition to the spectral complexity of the cD galaxy region. We do not detect any significant spatial temperature variations in AWM7, except around the cD galaxy, in agreement with the earlier *ASCA* analysis of this cluster. Radial temperature profiles of these two clusters are in a qualitative agreement with *ROSAT*. However, while *ASCA* average temperatures (5.5 and 3.9 keV, respectively) agree with those from other high-energy instruments (*Ginga* and *EXOSAT* for A3558 and *Einstein* MPC and *EXOSAT* for AWM7), *ROSAT* temperatures are lower by factors of 1.7 and 1.25, respectively. We find that including realistic estimates of the current *ROSAT* systematic uncertainties enlarges the temperature confidence intervals so that *ROSAT* measurements are consistent with others for these two clusters as well. Due to the limited energy coverage of *ROSAT* PSPC, its results for the hotter clusters are highly sensitive to calibration uncertainties. We conclude that within the present calibration accuracy, there is no disagreement between *ASCA* and other instruments. This adds confidence to the *ASCA* results on the hotter clusters which can at present be studied with precision only with this instrument. On the scientific side, a *ROSAT* temperature underestimate for A3558 may be responsible for the anomalously high gas to total mass fraction found by Bardelli et al. in this core member of the Shapley supercluster.

*Subject headings:* galaxies: clusters: individual (A2256, A3558, AWM7) — intergalactic medium — methods: data analysis — X-rays: galaxies

### 1. INTRODUCTION

In this paper, we focus on a comparison of *ASCA* and *ROSAT* spatially resolved temperature measurements of clusters of galaxies. Such measurements are of great importance; for example, they are needed for the determination of cluster masses, a problem which has fundamental cosmological implications (e.g., White et al. 1993). Resolved temperature measurements for a significant number of hot (and therefore most massive) clusters have only become possible now with the advent of *ASCA* with its imaging capability and the 0.5–11 keV energy coverage (Tanaka et al. 1994). Recent *ASCA* papers on several hot clusters have reported the detection of unexpectedly strong temperature gradients in the outer cluster regions in several cases (e.g., in A2163, A665, A2256, A2319, Markevitch et al. 1996; Markevitch 1996, hereafter M96; A2218, Loewenstein et al. 1996). These observations contradict the common assumption that clusters are isothermal. *ASCA* analysis techniques are relatively complex due to the properties

of the *ASCA* mirrors and at present are far from being established. Therefore, it is necessary to independently confirm the *ASCA* findings for at least those clusters for which other data are available. *ROSAT* PSPC data with good spatial resolution exist for many clusters. For the hotter objects, however, these data are only of limited use, due to the weak temperature dependence of the cluster spectrum shape within the PSPC 0.1–2.5 keV energy band, which means that any calibration uncertainty translates into a large error in the measured temperature, even for observations with good statistics. Nevertheless, some temperature estimates can be derived with *ROSAT*. Below we compare *ASCA* and *ROSAT* results on three clusters with different temperatures and either absent or weak cooling flows (to avoid complication of the *ASCA* analysis), for which there are published *ROSAT* results and publicly available *ASCA* data. These are the hot cluster A2256 ( $z = 0.058$ ), cooler, rich cluster A3558 ( $z = 0.048$ ) and the cool nearby group AWM7 ( $z = 0.018$ ). *ASCA* results on A2256 have been re-

<sup>1</sup>Also IKI, Profsoyuznaya 84/32, Moscow 117810, Russia

ported in M96; Churazov et al. (1996) obtained generally similar results using an independent technique. *ROSAT* data on A2256 have been previously analyzed by Briel & Henry (1994, hereafter BH) who found a temperature profile different from (although not inconsistent with) M96. BH also found two high-temperature regions in this cluster, whose existence was not confirmed by *ASCA* (M96). *ROSAT* results on A3558 have been reported by Bardelli et al. (1996, hereafter B96), while those on AWM7 were given by Neumann & Böhringer (1995, hereafter NB). Full analysis of the AWM7 *ASCA* observations was presented by Ohashi et al. (1994) and Ezawa et al. (1996), as well as by Loewenstein (1995). In this paper, we perform a detailed reanalysis of A2256 *ROSAT* PSPC data and discuss the sources of the apparent discrepancy with the results of BH. We also present the first analysis of *ASCA* data on A3558 and our independent reanalysis of the *ASCA* central pointing toward AWM7, as well as a brief reanalysis of *ROSAT* A3558 and AWM7 observations for which we confirm the results published earlier. In this paper, we discuss the values of the gas temperature projected onto the image plane (as opposed to those for three-dimensional cluster regions), to facilitate comparison with other work. A value of  $H_0=50 \text{ km s}^{-1} \text{ Mpc}^{-1}$  is used throughout the paper.

## 2. ROSAT ANALYSIS OF A2256

Six *ROSAT* observations of A2256 — a central exposure with the PSPC-C detector (June 1990) and five offset pointings with the PSPC-B (low gain state, October 1991–July 1992) — were analyzed by Briel et al. (1991) and BH. We reanalyze these data applying the updated calibration and a more accurate technique to obtain temperatures in the image annuli same as those used by M96 for *ASCA*. Since we intend to compare our results to those of BH, our analysis steps are given below with maximum detail. We accumulate spectra from the annuli  $r = 0-6-11-18-25'$  centered on the main cluster brightness peak. The regions containing the cooler infalling group (a  $90^\circ$  sector within  $r = 11'$ ) and the central galaxy (a  $2'$  radius region) detected by BH, are excluded to facilitate comparison with the M96 results which are largely insensitive to the presence of such cool substructure due to the higher energy band. Flat-fielded images in the energy bands of 0.20–0.42–0.52–0.70–0.91–1.32–2.01 keV, free of particle and most non-cosmic X-ray background, are generated using the approach and code of Snowden et al. (1994). Cosmic (including any residual non-cosmic) X-ray background is then calculated individually in each energy band and for each pointing, using image regions more than  $40'$  from the cluster center, within  $28-50'$  from the detector center and free of detectable sources. This results in a relative accuracy of the background normalization of about 5% (estimated by experimenting with different image regions). We then employ and compare two techniques to correct for the recently recognized SASS processing error (Snowden et al. 1995) which introduces spurious gain variations over the detector face. This error has especially serious implications for the results on clusters with temperatures above  $\sim 2.5$  keV, the *ROSAT* upper energy cutoff. The first method (method A hereafter) is to obtain cluster fluxes

directly from the flat-fielded images which are derived using the presently available detector efficiency maps (Snowden et al. 1994) affected by the same error in the same way, thus canceling the error to some extent (S. Snowden, private comm.) The fluxes are then fitted using the on-axis spectral response, binned in the broad energy bands. An advantage of this approach is that it automatically includes all non azimuthally-symmetric variations of the effective exposure, which are about  $\pm 10\%$  on a several-arcminute scale and are energy-dependent, as can be seen from comparison of the exposure maps for different energy bands. These variations are due to a combination of the spatial variations of the detector gain and efficiency. A disadvantage of this method is that the detector efficiency maps in the wide energy bands are, in fact, a convolution of the efficiency and the X-ray background spectrum, which may be different from the object spectrum. Another source of bias, which should be most prominent at large off-axis angles, is a combination of the poor detector energy resolution and the decline of the effective area with energy, such that the division of the detector count rate by the effective area artificially increases the flux at the highest energies — a 1 keV photon which is detected as 2 keV is being divided by the smaller effective area corresponding to 2 keV. Also, this method is not optimal for minimizing statistical uncertainties, since it assigns too high a weight to the outer regions with poorer statistics. It is therefore preferable to use a technique which convolves a model with the responses rather than attempting to deconvolve the data. In such a method (hereafter, method B), we correct the SASS gain error for each event using the code provided by the *ROSAT* team, generate flat-fielded images using S. Snowden's code, calculate and subtract the sky background, then multiply the background-subtracted images by the exposure maps (by which the raw images were divided for flat-fielding) and fit fluxes from these images. The model spectrum is multiplied by the azimuthally-symmetric off-axis area weighted by the cluster surface brightness within each region, and convolved with the binned photon redistribution matrix. The problems here are that at present there are no detector maps corrected for the SASS gain error so the background estimate may be less accurate, due to the spurious gain differences between the outermost detector area used to calculate the background and the central image area used for spectra (Snowden et al. 1995). Also, any azimuthally-asymmetric effective exposure variations that are not due to the SASS gain error, are ignored. Since neither method is fully satisfactory at present, we use both (with some additional variations), and include the residual calibration uncertainties as systematic errors. We will see that the accuracy of this first-order approximation correction for the known problems is adequate for the purpose of this paper.

The systematic errors are estimated as follows. The rms difference of the background normalizations from the SASS gain error-corrected and uncorrected data is about 15%. We accept it as a reasonable estimate of the inaccuracy due to the use of inconsistent detector efficiency maps, and assume a 15% error of the background in each energy band. This supersedes the 5% error due to the background calculation technique alone, mentioned above. The rms difference of the cluster fluxes in our annuli between the

TABLE 1  
RESULTS OF FITTING A2256 *ROSAT* PSPC DATA USING DIFFERENT METHODS

cluster annulus, arcmin	method A	method B <sup>1,2</sup>		method B <sup>1</sup>		method A <sup>3</sup>	method B <sup>3</sup>
	$T_e$ , keV	$T_e$ , keV	90%	fix $N_H$ , use 0.5–2 keV	90%	use all FOV	gain uncorrected
				$T_e$ , keV		$T_e$ , keV	$T_e$ , keV
0–6	7.6	9.3	6.9–25	8.8	5.9–17	8.5	6.1
6–11	8.8	7.5	4.4–18	7.4	5.0–14	10.0	7.6
11–18	3.9	3.3	2.2–6.2	3.8	2.6–6.2	5.4	3.9
18–25	2.1	1.8	1.2–11	1.7	1.1–7.3	5.1	2.6

<sup>1</sup> For these columns, the background error of 15% and a systematic flux error of 5% are included. For other columns, only a background error of 5% and no flux error are included.

<sup>2</sup> Temperatures from this column are shown in Fig. 1.

<sup>3</sup> These columns are included for comparison only; the values we consider “correct” are in the previous columns.

corrected and uncorrected data is about 5%. Therefore, we chose to use a systematic error in flux of 5% in each of our energy bands as a reasonable representation of the calibration uncertainties related to the use of the uncorrected detector efficiency maps in method A and ignoring the spatial detector efficiency non-uniformities in method B. This choice is somewhat arbitrary since the errors of methods A and B are likely to be different, but is acceptable as an order of magnitude estimate. We do not include an error component due to the presently uncorrected residual time-dependent PSPC gain variations (Snowden et al. 1995), but our conservative 5% flux error should encompass that effect as well. Results obtained using different spectral response matrices vary less than those from the different methods described here, so we do not include the systematic errors due to the response matrix uncertainties.

In all pointings, we use only the image area inside the detector support structure ring,  $\theta < 18'$  to calculate the cluster fluxes, to minimize the calibration uncertainties and the biases of method A. For comparison, we have also performed the fitting using the data uncorrected for the SASS gain error with symmetric off-axis areas (as in most earlier analyses), as well as using the whole field of view. The free fitting parameters for each image region were plasma temperature, Galactic absorption column and normalization. Different pointings at the same region were fitted simultaneously (without co-adding the data) using the response matrices appropriate for the particular detector and its gain state. For the outermost cluster annulus, two of the six exposures, both covering the same South-West sector of the ring, give unacceptably high  $\chi^2$ , and we chose to exclude them from the fit for this region. Including them does not change the best-fit temperature significantly (changing it from 1.8 to 2.8 keV). Results of all fits are listed in Table 1. The columns which we consider “correct” are those for methods A with  $\theta < 18'$  and B with the SASS gain error corrected. Other two columns are included for comparison. We chose to use method B as our preferred method to calculate temperatures in the wide annuli for which the detector efficiency non-uniformities are likely to average out. If  $N_H$  is fixed at  $5 \times 10^{20} \text{ cm}^{-2}$  (the value consistent with all regions) and only the upper four energy intervals are fitted using this method, the temperatures remain unchanged, as is shown in the table. Fig. 1 shows results from our preferred method with confidence

intervals calculated including only 5% background error and no systematic flux error (solid) and 15% background plus 5% flux errors (dashed extensions), the best-fit values corresponding to the larger intervals. For the brighter and hotter inner regions the flux uncertainty is most important, while for the outer annulus it is the background uncertainty. Separate fits to different pointings are shown in Fig. 1 *b* and *c*.

Results from our “correct” methods, and even all but one best-fit value from the “incorrect” methods in Table 1, are well within the 90% one-parameter confidence intervals shown for our preferred method. This suggests that our systematic error estimates are adequate. This also suggests that use of the presently unavailable self-consistent calibration data to correct for the gain and detector efficiency variations, will not qualitatively alter our results, since our two methods use a reasonable approximation to correct for these effects. Calibration improvements will reduce the values of the systematic errors that need to be included.

### 2.1. Comparison with earlier *ROSAT* results

Fig. 1 shows that our *ROSAT* and *ASCA* temperature profiles are in excellent agreement, and *ROSAT* results even suggest that the temperature decrease found by *ASCA* continues at still larger radii. However, earlier *ROSAT* results obtained by BH from the same data are different (although only at about a 90% significance). We summarize the differences between BH and our analysis techniques which may be responsible for the discrepancy, in addition to the correction of the SASS spatial gain error.

1. Use by BH of the whole field of view and division of each count by a vignetting factor. The problems of this approach, included in the discussion of our method A above, are spurious enhancement of the high-energy flux at large off-axis angles and assignment of too much weight to low-statistics data. As Table 1 shows, inclusion of the outer detector area noticeably increases the best-fit temperatures, which may also be partially due to the less accurate effective area calibration there.

2. Gain adjustment. BH adjusted the PSPC gain in each pointing so that their overall cluster temperature becomes 7.5 keV, the value obtained by *Ginga*. We note that in the presence of cool substructure, this should introduce an error. Indeed, assuming after Briel et al. (1991) that

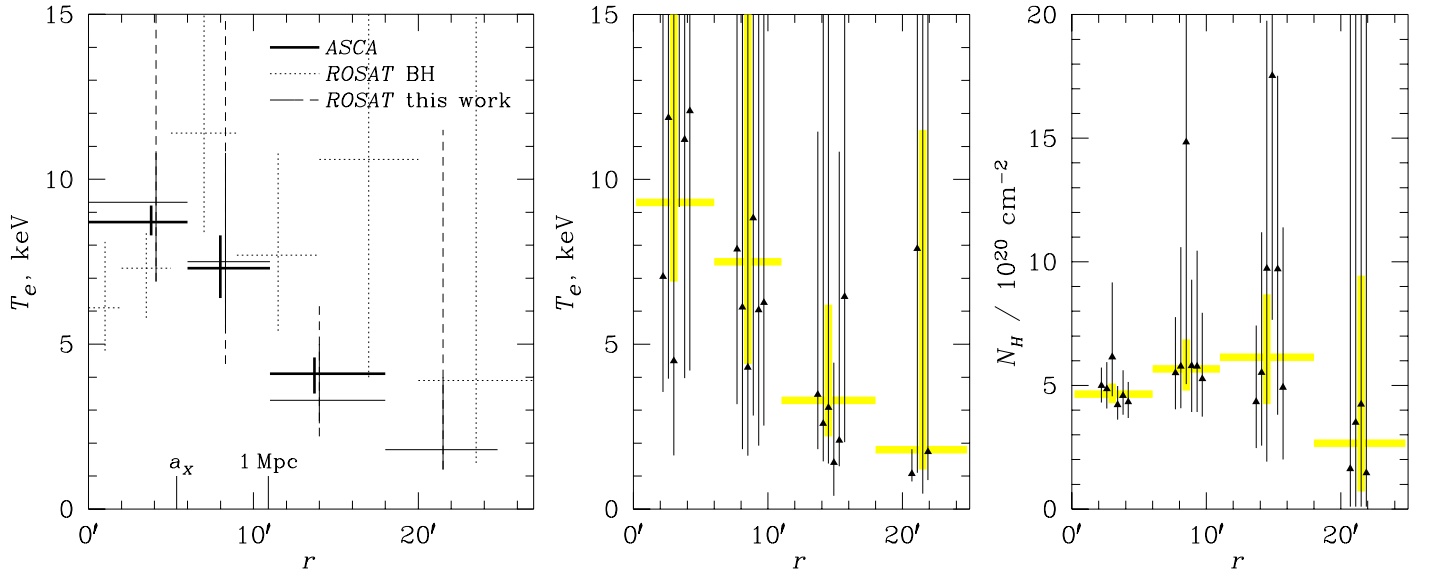


FIG. 1.—(a) Projected temperature profiles of A2256 from *ASCA* (Markevitch 1996) and *ROSAT* (BH and J. P. Henry, private comm.; this work) with 90% confidence intervals (BH’s 68% intervals are multiplied by 1.65). *ASCA* and our *ROSAT* analysis exclude from the first and second annuli cooler regions of the infalling group and (for *ROSAT*) the central cluster galaxy, found by BH. Values from BH are for the entire annuli, thus they are not directly comparable to ours in the inner  $10'$ . Dashed extensions of our *ROSAT* error bars show the effect of inclusion of the systematic errors. (b,c) Values of temperature and hydrogen column density for individual *ROSAT* pointings in our analysis for the same regions as in panel (a). Gray lines show values for all pointings fitted simultaneously, as in panel (a). There is no significant radial trend in  $N_H$ , even without inclusion of the systematic errors (such a trend, if existed, might indicate deficiencies of our analysis procedure), while there is a trend for the temperature to decrease with radius, in agreement with *ASCA*.

the cool subgroup has  $T_e = 2$  keV and contributes about 1/6 of the flux, while the rest of cluster has  $T_e = 8$  keV, *Ginga* should derive a 7.2 keV single-temperature fit while *ROSAT* would find 5.7 keV because of the different spectral coverage. We have not performed any gain adjustments but excluded the group region from our analysis.

3. Use of photons up to 2.5 keV. Our analysis is restricted to  $E < 2.0$  keV. According to the *ROSAT* User’s Guide, the calibration is not reliable above that energy, with the expected discrepancy between the model and data reaching 20%.

4. Summation of data from pointings which are performed with different detectors. We have fitted different pointings simultaneously but without co-adding the data, making use of the information on the detector identity and their differing properties.

We have also fitted the temperatures in the regions of the hot spots found by BH which lie  $7'$  to the North-East and South-West of the cluster center. Using method A to account for the non-uniformities of the detector efficiency, and including data within  $\theta = 18'$  from the detector center, we obtain temperatures of 8.8 ( $>4.4$ ) keV (90% interval) and 11.1 ( $>5.3$ ) keV for the more significant NE spot and less significant SW spot, respectively, if  $N_H$  is free, and 14.6 ( $>6.9$ ) keV and 4.8 (3.2–8.2) keV if it is fixed. No systematic errors were included except for the 5% background error, and inclusion of the flux error makes confidence intervals even larger. Our other methods give different best-fit values but never significantly different from the cluster mean. The SASS gain error correction reduces the temperature of the NE spot and increases that of the SW

spot. Inclusion of  $\theta > 18'$  data (which for these regions means offset pointings) changes the best-fit temperatures to 12.5 (5.6–24) keV and 14.5 (6.9–23) keV for the NE and SW spots, respectively, if  $N_H$  is a free parameter, and to 18.3 (8.7–24) keV and 6.0 (4.2–9.2) keV if it is fixed. We note, however, that these spots fall on the PSPC detector support ring in three (four) offset pointings out of five for the NE (SW) spots. We conclude that the hot spots reported by BH are probably artifacts.

### 3. A3558

#### 3.1. *ASCA* results

We restrict our present discussion to a comparison of results from *ASCA* and other instruments; a scientific interpretation will be presented elsewhere. We have analyzed the GIS and SIS data simultaneously to maximize statistical significance of the results, even though the SIS  $22' \times 22'$  field of view does not cover the whole cluster. The useful exposure for A3558 is 17 ks for the GIS and 12 ks for the SIS (which was operated partly in the 4-CCD mode and partly in the 2-CCD mode). To obtain a two-dimensional temperature map and a radial temperature profile of this cluster, we followed the technique of Markevitch et al. (1996) and M96 with some modifications regarding the central region. This technique consists of simultaneous fitting of the temperature in all image regions, taking into account the *ASCA* energy-dependent mirror scattering. The mirror PSF was modeled using Cyg X-1 data for energies above 2 keV (Takahashi et al. 1995). Unlike the clusters considered in M96, A3558, as well as

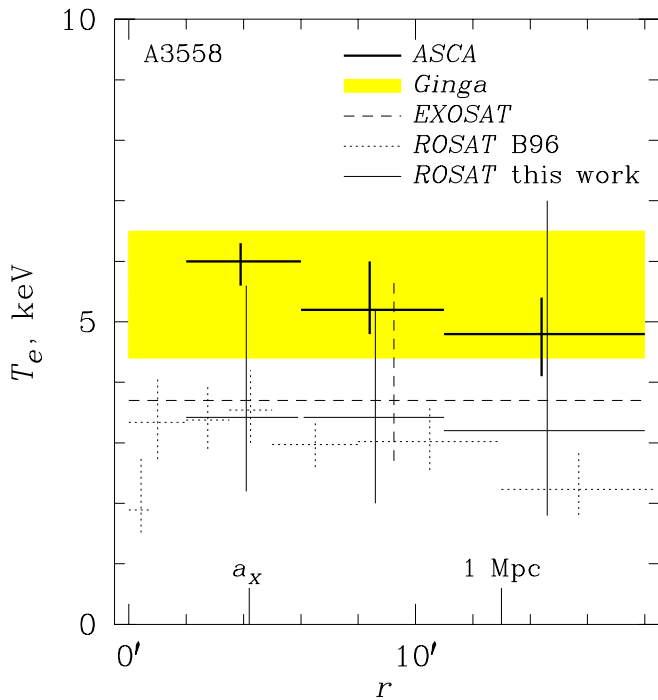


FIG. 3.—Projected temperature profiles of A3558 from *ASCA* (this work), *ROSAT* (B96 and this work), and the overall temperature from *Ginga* (Day et al. 1991) and *EXOSAT* (Edge & Stewart 1991). Errors are 90% confidence. The gray band shows the temperature range of the *Ginga* main spectral component for different models considered by Day et al. *ASCA* annuli are centered as shown in Fig. 2 (while they are narrower than those in Fig. 2). The core radius is estimated excluding the cD galaxy (B96). The *ASCA* single-temperature fit to the central region is 5.6 keV; however, its spectrum requires more than one component (see the text) and is not directly comparable to the *ROSAT* single-temperature fit. Our *ROSAT* values are similar to those from B96 when no systematic errors are included. Inclusion of systematic errors (shown) considerably enlarges the confidence intervals.

AWM7, have a central dominant galaxy and a cooler component in the center, known e.g., from the *ROSAT* data (below). Also, average temperatures of these clusters are lower. Therefore, it is desirable to include energies below 2.5 keV, which were excluded by M96 due to the PSF and other uncertainties. In the present analysis, we use energies starting from 1.5 keV (excluding the poorly calibrated 2–2.5 keV interval). For energies below 2 keV, the PSF data from the 2–3 keV interval were used after the appropriate correction for the energy dependence of the GIS spatial resolution. Comparison of this extrapolation of the PSF model to the brightness profile of a point source as in Takahashi et al. shows that its inaccuracy is less than 10% for the interesting range of radii. We use this value as a relative PSF uncertainty in the annuli, while assuming a 15% uncertainty for sectors during the temperature map reconstruction. As in M96, we use a *ROSAT* PSPC image as the surface brightness template, correcting it for the non-isothermality under the assumption that the projected temperature is constant over each region, with the exception of the region around the cD galaxy. For these central regions with a possibly complex spectrum, this technique is inadequate and the model relative normalization (set by the *ROSAT* image for other regions) is fitted as a free

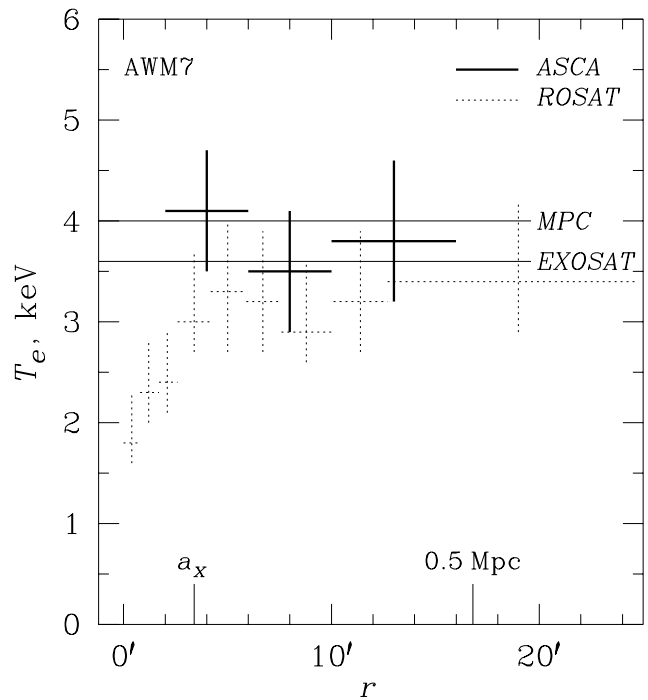


FIG. 4.—Projected temperature profiles of AWM7 from *ASCA* (this work), *ROSAT* (NB) and the overall temperature from the *Einstein* IPC (David et al. 1993) and from *EXOSAT* (Edge & Stewart 1991). Errors are 90% confidence. Annuli are centered on the cD galaxy. The core radius is from an estimate excluding the cD galaxy (NB). The *ASCA* temperature value for the cD galaxy region (3.9 keV single-temperature fit) is discussed in the text. *ROSAT* values outside the cD region are systematically lower than those from other instruments.

parameter together with the temperatures.

B96 who analyzed *ROSAT* data on A3558, found that the cD galaxy peak is displaced by 1.3' with respect to the centroid of the surrounding cluster. We centered our inner region on the cD galaxy but all other rings on the cluster centroid, both for the map and the profile analysis. Our resulting temperature map overlaid on the *ROSAT* image is shown in Fig. 2. Sectors of the annuli in Fig. 2 were chosen to sample the cluster regions approximately parallel and perpendicular to the possible merger direction (see the image). Projected temperatures in the annuli with  $r = 2 - 6 - 11 - 18'$  are shown in Fig. 3 (such angular resolution is at the limit of *ASCA* capabilities at the present calibration accuracy). There is a nearby poor cluster  $\sim 25'$  to the East of A3558 and another one still farther in the same direction (Breen et al. 1994; B96). A sector containing part of the nearby cluster was included in the analysis to account for the scattering of its flux especially into our region 9 (Fig. 2), although its contribution was found to be negligible. Its temperature was fixed at 4 keV. The stray light contribution from these sources is negligible because of their low flux and the favorable value of the telescope roll angle used in this observation (Ishisaki 1996).

In the cD galaxy region, a single-temperature fit re-

sults in  $T_e = 5.6$  keV and  $\chi^2 = 270$  with 256–14 d.o.f. (for the simultaneous fit of the spectra from the annuli). The fit is significantly improved if an additional spectral component is allowed in the central region. For a simple model consisting of two thermal components, we obtain the temperatures<sup>2</sup> of  $1.1_{-0.3}^{+0.6}$  keV and 12 ( $> 8$ ) keV with approximately equal projected emission measure in the  $r = 2'$  cD galaxy region (this region has about a quarter of the total cluster emission measure), and  $\chi^2 = 240$  with 256–16 d.o.f. This model is consistent with the ROSAT PSPC single-temperature fit to the same region. A power-law second component fits the data equally well ( $\chi^2=245$ ) but the resulting photon index is unphysical (+0.5). A power law with the index fixed at the typical AGN value of  $-1.7$  improves the fit less significantly. A more detailed analysis and discussion will be presented elsewhere; here we only note that there definitely is some hard spectral component in the central region, because there is excess flux in that region at the highest ASCA energies.

Using different models for the central region does not change the results for the rest of the cluster considerably. There is a significant asymmetric temperature pattern in the map (Fig. 2), with the North-East sector of the cluster hotter than other regions. The temperature values in regions 2-9 could not be due to statistical deviations from the same mean at the 99.9% confidence; the temperatures in regions 2-5 of the second annulus are different at the 98% confidence. The results of fitting SIS and GIS data separately are in good agreement, and this temperature pattern is present in both fits. There is also a slight radial decline of the cluster temperature (Fig. 3), although it is marginally significant. We obtained an average cluster temperature of  $5.5_{-0.2}^{+0.3}$  keV.

### 3.2. Comparison with other instruments

A3558 was observed by EXOSAT (Edge & Stewart 1991) in an offset pointing from which a poorly constrained temperature of  $3.8_{-1.0}^{+2.0}$  keV was obtained. Day et al. (1991) reported a Ginga overall temperature of  $5.7 \pm 0.2$  keV for this cluster and found that the spectrum requires more than one component. Additional components they considered were a power law with  $\gamma = -1.7$  or a cooler gas, which both significantly improved the fit. ASCA results presented above are in good agreement with these measurements. ROSAT PSPC data were analyzed by B96 who obtained a significantly lower temperature of  $3.3_{-0.3}^{+0.4}$  keV for the inner  $r = 5'$  excluding the cD galaxy and a slight decrease of the temperature outward. B96 discussed their inconsistency with Ginga and suggested that the Ginga wide-aperture flux may be contaminated by emission from nearby clusters. We note that, although the Ginga field of view included the nearest clusters, they are far less luminous and are expected to be cooler as well. Therefore, they are unlikely to produce such a temperature overestimate. We have reanalyzed the ROSAT data and obtained results almost identical to those from B96, using our method B without the SASS gain error correction and not including the systematic errors to facilitate comparison. The SASS error correction did not change the temperature values noticeably for this observation. However, if the systematic

errors like those we used above for A2256 are included, the error bars are increased sufficiently so that the results become consistent with ASCA and Ginga within the 90% confidence intervals. Indeed, to raise the PSPC-derived temperatures to the ASCA values, only a 7–8% increase in the flux is necessary in our highest PSPC energy band. Our ROSAT values for the same outer three annuli used in the ASCA analysis, including the systematic errors, are shown in Fig. 3. Note that the systematic errors are not of statistical nature and may not necessarily be reduced by averaging over the entire cluster. They will be reduced by improvements in the calibration. One of such calibration-related errors is a possible anomalous PSPC gain in this particular observation (performed in July 1991 with PSPC-B in high gain state) which may drive all best-fit temperatures down. A gain change of 3% would suffice to produce the observed discrepancy. It is unlikely that any correction for this effect would drastically change the radial temperature distribution. Except for the absolute values, the ASCA and ROSAT projected temperature profiles in Fig. 3 both are consistent with a slightly decreasing temperature, outside the central region. We note that the anomalously high gas to total mass fraction in this cluster, obtained by B96 using the ROSAT temperatures for the total mass calculation, may be overestimated by a factor of about 1.7 because of this temperature uncertainty.

### 4. AWM7

This nearby poor cluster was observed by ASCA with several offset pointings. The complete dataset is analyzed by Ezawa et al. (1996), who included a detailed treatment of stray light contamination which is important for off-set pointings. Earlier, the central pointing was analyzed by Ohashi et al. (1994). These authors found that the gas temperature in this cluster does not change with radius but a cooler component and an abundance increase is required in the central region containing the cD galaxy. Here we limit our analysis to only the central pointing for which the stray light is unimportant, and derive a two-dimensional temperature distribution and a radial temperature profile out to  $16'$  from the cluster center, using the same method as in Section 3. For this cluster, only GIS data are used for simplicity, which is sufficient for the technical purpose of this paper. For the  $r = 0 - 2 - 7 - 16'$  annuli centered on the cD galaxy and the outer 2 rings divided into 4 (or 5) sectors, we detect no significant temperature deviations from the cluster average of  $3.9 \pm 0.2$  keV. ASCA temperatures in the narrower,  $r = 2 - 6 - 10 - 16'$  concentric annuli are presented in Fig. 4. Since the cluster emission is present beyond our outermost annulus, the ROSAT emission to  $r = 20'$  from the cluster center is included in the model for the last ring (both for the map and the profile analysis) to avoid boundary effects. Our temperature profile is consistent with an isothermal one, similarly to the Ezawa et al. results in the same range of radii. The single-temperature models for all regions are acceptable; in the central  $r = 2'$  region, our single temperature is  $3.9 \pm 0.7$  keV. However, if lower energies starting from 0.7 keV are included in our analysis (only for this estimate), the addi-

<sup>2</sup>Errors are 90% single-parameter confidence intervals throughout the paper. ASCA errors are estimated by simulations including systematic uncertainties.

tion of a cooler component in the region of the cD galaxy improves the fit. For two thermal components, the best-fit temperatures are  $4.8_{-0.9}^{+1.8}$  keV and  $1.3 \pm 0.3$  keV with the cool component contributing a fraction of the projected emission measure within  $r = 2'$  equal to  $0.24 \pm 0.12$ . This model is consistent with the *ROSAT* single temperature fit in the same region.

Fig. 4 also shows results from two other high energy but spatially unresolved observations of this cluster, with the *Einstein* MPC (David et al. 1994) and *EXOSAT* (Edge & Stewart 1991). *ASCA* agrees well with both instruments. Also shown in the figure is the *ROSAT* PSPC temperature profile obtained by NB from the observation performed in January 1992 (PSPC-B low gain state). This profile lies systematically below all three high-energy measurements even outside the cooler cD galaxy region, although the temperatures in individual radial bins are consistent with them within the 90% confidence intervals. Including only the 5% systematic background error, we obtained an average *ROSAT* temperature of  $3.1 \pm 0.2$  keV for the cluster excluding the  $r = 3'$  central region and the area outside  $\theta = 18'$ . This value is similar to the median value of the temperature profile from NB but is significantly below the values from other instruments. However, the discrepancy is less prominent than that for A3558 discussed above. The same systematic error as that used above, is certainly sufficient to account for the difference. Both *ASCA* and *ROSAT* profiles agree in that there is no significant temperature change with radius outside the cD galaxy region. Note that for this nearby galaxy group, our measurements cover a much smaller linear size at the group's distance than for other clusters studied.

## 5. SUMMARY

We have presented a reanalysis of the *ROSAT* PSPC observations of A2256 and of the *ASCA* central pointing of AWM7, as well as first *ASCA* results on A3558. Our primary goal has been to compare *ASCA* cluster temperatures with those from other instruments; thus, we have focused on the technical issues of data analysis rather than physical interpretation. We find that:

1. The *ROSAT* data on A2256 are in excellent agree-

ment with recent *ASCA* findings (M96), including the detection of the temperature decline with radius, although with much larger errors than those of *ASCA*. Hot gas regions earlier reported by BH from the *ROSAT* data are probably artifacts;

2. The *ROSAT* and *ASCA* temperature profiles for A3558 and AWM7 qualitatively agree. For AWM7, there is no significant temperature variations with radius outside the cD galaxy region. For A3558, there is a slight radial temperature decline outside the central region. For the cD galaxy regions, the instruments agree when a multi-temperature spectrum is allowed;

3. *ASCA* values of the overall temperature for A3558 and AWM7 (5.5 and 3.9 keV, respectively) are in agreement with those derived by other high-energy instruments. However, the *ROSAT* absolute temperature values for these clusters are lower. We note that, although formally statistically significant, the discrepancy is within the current *ROSAT* calibration uncertainties, which we propose as its likely cause.

These findings add confidence in the *ASCA* results on other clusters, for which *ASCA* is the only instrument capable of mapping the spatial temperature distribution. They also underline the high sensitivity of the *ROSAT* temperature measurements for hot clusters to the calibration uncertainties. We also find that:

4. *ASCA* two-dimensional temperature map of AWM7 (within  $r < 16'$ ) does not display any significant spatial temperature variations outside of the cD galaxy regions. An asymmetric temperature pattern is found in A3558;

5. From *ASCA* data, the central region of A3558 contains a source of emission harder than the cluster average and perhaps harder than the typical AGN power law emission, in addition to a cooler component.

This work was motivated by discussions at the "X-ray Imaging and Spectroscopy" conference held in Tokyo in March 1996. We thank Steve Snowden for a useful discussion regarding the *ROSAT* calibration, and Bill Forman and Craig Sarazin for valuable comments on the manuscript. MM was supported by NASA grants NAG5-2526 and NAG5-1891. AV received support from the Smithsonian Institution.

## REFERENCES

- Bardelli, S., Zucca, E., Malizia, A., Zamorani, G., Scaramella, R., & Vettolani, G. 1996, *A&A*, 305, 435
- Breen, J., Raychaudhury, S., Forman, W., & Jones, C. 1994, *ApJ*, 424, 59
- Briel, U. G., et al. 1991, *A&A*, 246, L10
- Briel, U. G., & Henry, J. P. 1994, *Nature*, 372, 439 (BH)
- Churazov, E., Gilfanov, M., Forman, W., & Jones, C. 1996, in "X-ray Imaging and Spectroscopy of Cosmic Plasmas", ed. F. Makino, in press
- Day, C. S. R., Fabian, A. C., Edge, A. C., Raychaudhury, S. 1991, *MNRAS* 252, 394
- David, L., Slyz, A., Jones, C., Forman, W., Vrtilik, S. D., & Arnaud, K. A. 1993, *ApJ*, 412, 479
- Edge, A. C., & Stewart, G. C. 1991, *MNRAS*, 252, 414
- Ezawa, H., Fukazawa, Y., Haiguang, X., Kikuchi, K., Makishima, K., Ohashi, T., Tamura, T., Yamasaki, N. 1996, in "X-ray Imaging and Spectroscopy of Cosmic Plasmas", ed. F. Makino, in press
- Ishisaki, Y. 1996, PhD thesis, University of Tokyo
- Loewenstein, M., 1995, presented by R. Mushotzky in "Röntgenstrahlung from the Universe", eds. H. U. Zimmermann et al., MPE Report 263
- Loewenstein, M., Mushotzky, R., & Donahue, M. 1996, in "X-ray Imaging and Spectroscopy of Cosmic Plasmas", ed. F. Makino, in press
- Markevitch, M., Mushotzky, R. F., Inoue, H., Yamashita, K., Furuzawa, A., & Tawara, Y. 1996, *ApJ*, 456, 437
- Markevitch, M. 1996, *ApJ*, 465, L1 (M96)
- Neumann, D. M., & Böhringer, H. 1995, *A&A*, 301, 865
- Ohashi, T., et al. 1994, in "New Horizon of X-ray Astronomy", eds. F. Makino & T. Ohashi (Tokyo: Universal Academy)
- Snowden, S. L., McCammon, D., Burrows, D. N., Mendenhall, J. A. 1994, *ApJ*, 424, 714
- Snowden, S. L., Turner, T. J., George, I. M., and Yusaf, R. 1995, OGIP Calibration Memo CAL/ROS/95-003
- Takahashi, T., Markevitch, M., Fukazawa, Y., Ikebe, Y., Ishisaki, Y., Kikuchi, K., Makishima, K., & Tawara, Y. 1995, *ASCA Newsletter*, # 3 (NASA/GSFC)
- Tanaka, Y., Inoue, H., Holt, S. S. 1994, *PASJ* 46, L37
- White, S. D. M., Navarro, J. F., Evrard, A. E., & Frenk, C. S. 1993, *Nature*, 366, 429

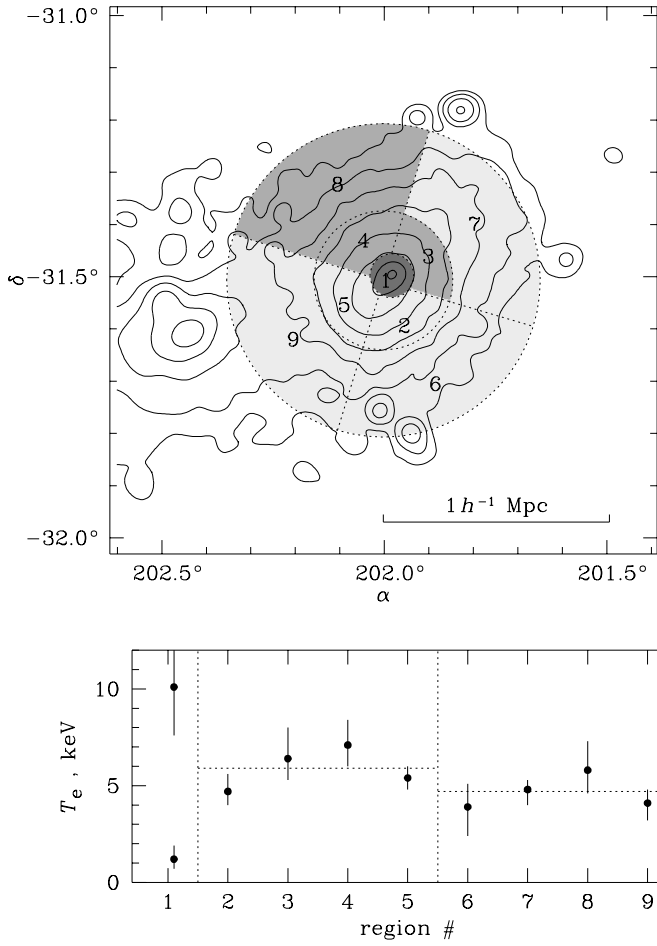


FIG. 2.—*ASCA* temperature map of A3558. Contours are *ROSAT* surface brightness and dashed lines are boundaries of the regions in which the *ASCA* temperature is reconstructed. The inner  $r = 2.5'$  circle is centered on the cD galaxy while other rings ( $8'$  and  $18'$ ) are centered on the cluster centroid determined by B96. The temperatures are shown by grayscale (hotter is darker). Regions are numbered and their temperature values with 90% confidence intervals are shown in the lower panel. For the central region, the result of a two-temperature fit is shown (see the text), and the grayscale arbitrarily corresponds to the higher-temperature component. Dashed horizontal lines in the lower panel show average temperatures in each ring.